Microbial-inspired antidotes to repurpose toxic compounds as antibiotics

AUTHORS: Tahoura Samad[1,7], Chayanon Ngambenjawong[1,5], Henry Ko[1], Savan Patel[6], Cristiana DeAgazio[1], Heather E. Fleming[1,2,8], Sangeeta N. Bhatia[1,2,4,6,7,8]

AFFILIATIONS:

1. Koch Institute for Integrative Cancer Research, Massachusetts Institute of Technology, Cambridge, MA 02139
2. Marble Center for Cancer Nanomedicine, Massachusetts Institute of Technology, Cambridge, MA 02139
3. Department of Biology, Massachusetts Institute of Technology, Cambridge, MA 02139
4. Department of Electrical Engineering and Computer Science, Massachusetts Institute of Technology, Cambridge, MA 02139
5. School of Biomolecular Science and Engineering, Vidyasirimedhi Institute of Science and Technology (VISTEC), Rayong, Thailand
6. Harvard-MIT Division of Health Sciences and Technology, Cambridge, MA 02139
7. Institute of Medical Engineering and Science, Massachusetts Institute of Technology, Cambridge, MA 02139
8. Howard Hughes Medical Institute, Massachusetts Institute of Technology, Cambridge, MA 02139

ABSTRACT:

Antibiotic-resistant (AMR) bacterial infections are a major global health threat. Despite the critical need for new antimicrobials, progress is constrained by protracted development timelines, as well as the requirement for chemical novelty to avoid cross-resistance. Repurposing therapeutics approved for indications other than infection offers a potential shortcut to rapidly develop new antibiotics that are outside of existing antibiotic classes and therefore less susceptible to resistance. Cancer therapeutics, which often disrupt essential cellular processes that are evolutionarily conserved within bacteria, are a promising source of novel antimicrobial candidates. However, the narrow therapeutic index of these compounds limits their application for infection. Here, we establish a two-component strategy to repurpose highly toxic therapeutics as antimicrobials by improving their safety profile, using the cytotoxin calicheamicin as a proof-of-concept. In the first arm, we engineer a conditionally-active drug conjugate that restricts calicheamicin activity to infected tissue, improving its therapeutic index. In the second arm, we administer a re-engineered self-resistance enzyme from *Micromonospora echinospora*, the natural producer of calicheamicin, as an “antidote” to neutralize calicheamicin released outside of infected tissue, further widening its therapeutic index. The calicheamicin conjugate exhibits activity against a panel of Gram-negative and Gram-positive pathogens in response to a protease present within the infected microenvironment. Delivered in combination with the antidote, we demonstrate that antibacterial efficacy is maintained, and off-target toxicity is reduced in a mouse model of bacterial pneumonia. We anticipate that our dual strategy, which enhances drug safety by combining conditional activation of drug activity with neutralization of off-target effects, provides a generalizable framework for repurposing other promising but toxic compounds as antimicrobials.

INTRODUCTION:

Antimicrobial-resistant (AMR) infections are a critical health threat. The World Health Organization (WHO) estimates that resistance to existing drugs directly caused 1.27 million deaths globally and contributed to an additional 4.95 million deaths in 2019 (*1*). Development of new agents to address AMR infections is slow, hindered by the lengthy and costly processes of drug discovery and regulatory approval (*2*), and further challenged by cross-resistance, in which newly developed compounds that are similar to antibiotics are subject to the rapid development of resistance(*3*). Additionally, the economics of antibiotic treatment, which can involve short courses of treatment and stewardship programs to limit use, disincentivize investment in antimicrobial development by industry (*2*). Together, these scientific, regulatory, and economic hurdles have resulted in a widening gap between the rise of AMR and the pace of antibiotic development. Given this landscape, there is a critical need for innovative approaches to create antibiotics rapidly, while introducing novel mechanisms of action that help insulate against cross-resistance.

Current methods to develop new antibiotics often involve high throughput screening of small molecule libraries against predicted antimicrobial targets or whole cells. While tools such as machine learning (*4*–*7*), large-scale chemical-genetics (*8*), computational modeling of compound-target interactions (*9*), and genome mining (*10*, *11*) have greatly enhanced this process, promising lead compounds still face a prolonged and expensive development pipeline. Screening for companion compounds that can amplify the effectiveness of existing antibiotics (*9*, *12*) or mitigate drug resistance (*13*) is another strategy to accelerate drug development and has yielded notable successes, such as Augmentin (*13*, *14*). However, the use of existing antibiotics in these combination approaches may still leave them vulnerable to common resistance mechanisms (*13*). Alternatively, leveraging drugs approved by regulators for conditions other than infection, known as drug repurposing, might offer a pool of antibiotic candidates that are distinct

76 from existing approved antimicrobials while also shortening the development timeline (*15*).
77 Cancer therapeutics, many of which disrupt fundamental, conserved biological processes such
78 as DNA replication and metabolism, are a rich source of compounds with potential antimicrobial
79 activity. However, the narrow therapeutic index of these agents—the difference between the
80 effective therapeutic dose and the dose that causes substantial toxicity (Fig. 1A)—limits their
81 direct translation for infectious disease applications. Toxicities routinely tolerated in oncology,
82 such as myelosuppression (*16*), neuropathy (*17*), or even secondary malignancies (*18*), would be
83 unacceptable for patients with acute infections, who are frequently otherwise healthy.
84 Repurposing chemotherapeutic agents for antimicrobial use will therefore require innovative
85 strategies to widen their therapeutic index.

86 In this study, we present a two-armed, generalizable strategy for repurposing toxic
87 compounds as antimicrobials by widening their therapeutic index. As a proof-of-concept, we
88 apply this strategy to calicheamicin, a potent DNA-damaging agent that is approved for cancer
89 treatment, but which causes significant hepatotoxicity that would preclude administration to
90 patients with infections (*19*, *20*). In the first arm of our approach, we formulate calicheamicin as
91 a conditionally-active conjugate, adapting design principles that have been used to deliver
92 potent cytotoxic payloads in oncology (17,18). In this format, we tether calicheamicin to a
93 carrier protein through a protease-cleavable linker. While conjugated, the cytotoxic activity of
94 calicheamicin is masked until an infection-associated protease releases the drug, thereby
95 confining activity to infected tissue and reducing toxicity to healthy tissue, widening the
96 therapeutic index (Fig. 1B). Recognizing that even limited exposure of healthy tissue to a
97 compound as potent as calicheamicin can cause severe damage, we introduced a second arm
98 into our strategy to neutralize any drug released or diffusing beyond the infection site**.** To this
99 end, we adapted a natural microbial strategy, the self-resistance mechanism of
100 *Micromonospora echinospora,* the natural producer of calicheamicin*. M. echinospora* produces

101 several enzymes that neutralize calicheamicin to protect itself from autotoxicity (*21*, *22*); we
102 hypothesized that we could engineer and administer these enzymes as “antidotes” to neutralize
103 off-target calicheamicin, further widening the therapeutic index (Fig. 1C). We first show that our
104 calicheamicin-containing drug conjugate exhibits activity dependent on an infection-associated
105 protease against a panel of Gram-negative and -positive priority pathogens, and that prior to
106 cleavage, this conjugated format masks calicheamicin toxicity to mammalian cells. We further
107 show that bacterial-derived calicheamicin self-resistance enzymes can be re-engineered to act
108 as long-circulating "antidotes" that neutralize off-target calicheamicin *in vitro* and *in vivo*,
109 reducing liver toxicity. Finally, we validated that the combination of these two strategies
110 achieves therapeutic efficacy in a mouse model of pneumonia and reduces systemic toxicity.
111 Our dual approach provides a modular framework for the rapid repurposing of other promising-
112 yet-toxic natural products for use as antibiotics.

113 **RESULTS**

114 **Calicheamicin has broad spectrum activity against Gram-positive and Gram-negative**
115 **pathogens**

116 We first evaluated the antimicrobial activity of calicheamicin against a panel of Gram-
117 negative and Gram-positive bacterial pathogens, including several designated as priority
118 pathogens by the World Health Organization (*23*). Measuring microbial susceptibility to
119 calicheamicin using broth microdilution assays, we determined the minimum inhibitory
120 concentration (MIC) of calicheamicin across representative strains (Table 1). We found that
121 calicheamicin had potent activity against the Gram-positive bacterium *Staphylococcus aureus*,
122 with an MIC of 0.0006 μg/mL, a potency that was comparable to or greater than that of a
123 clinically used antibiotic vancomycin (Table 1). Notably, this potency was maintained against a
124 methicillin-resistant *S. aureus* (MRSA) isolate, BA1556. Calicheamicin also demonstrated

activity against Gram-negative pathogens including *Pseudomonas aeruginosa*, *Escherichia coli*, and *Klebsiella pneumoniae*, with MIC values ranging from 0.015 to 0.5 μg/mL (Table 1). Together, these data demonstrate that calicheamicin exhibits broad-spectrum antimicrobial activity, with efficacy extending to multidrug-resistant strains, and at concentrations that would be realistic for clinical translation.

Conditionally-active calicheamicin conjugate masks cytotoxicity while retaining antibacterial activity *in vitro*

While the potent antimicrobial activity of calicheamicin is a promising starting point, its substantial toxicity toward mammalian cells, particularly liver cells, precludes its use as a free compound. In oncology, this limitation has been addressed by formulating calicheamicin as an antibody–drug conjugate (*24*, *25*), where targeting and conditional activity improve the therapeutic index. Building on this approach, we developed a conditionally-active calicheamicin conjugate tailored for the infection context. In this design, calicheamicin was tethered to an albumin-binding domain (ABD) via a protease-sensitive linker that masks its cytotoxic activity until cleavage by infection-associated proteases (Fig. 2A). Use of albumin as the carrier protein leverages endogenous trafficking pathways to enhance accumulation (*26*, *27*) , retention (*28*), and mucopenetration (*29*) at sites of infection. As a linker between albumin and the drug, we used a peptide sequence cleavable by neutrophil elastase, which is enriched at sites of bacterial infection due to immune cell recruitment.

To generate the ABD–calicheamicin conjugate (ABD-Cal), we prepared a calicheamicin–peptide intermediate and coupled it to a recombinantly-expressed ABD using strain-promoted azide–alkyne cycloaddition. We next tested whether conjugation masked the cytotoxic activity of calicheamicin and allowed for protease-dependent activation by assessing antibacterial activity and mammalian cell toxicity in the presence or absence of neutrophil elastase *in vitro*.

149 The conjugate was incubated with neutrophil elastase or vehicle control for 4 hours prior to
150 evaluation. We then measured antibacterial activity against a representative Gram-positive (*S.*
151 *aureus*) (Fig. 2B) and Gram-negative (*K. pneumoniae*) pathogen (Fig. 2C). In the absence of
152 protease, we observed no antimicrobial activity; in the presence of protease, we observed a
153 recovery in antimicrobial activity with a (~60-120-fold) change in the minimum inhibitory
154 concentration (MIC) between the intact and cleaved conjugates, depending on the pathogen
155 tested. We also assessed whether formulation of calicheamicin as a conditionally-active
156 conjugate protected mammalian cells from toxicity. We found that in the absence of protease,
157 the intact conjugate demonstrated minimal mammalian toxicity to HepG2 liver cells after 24
158 hours of exposure (Fig. 2D). Together, these data show that calicheamicin, when formulated as
159 a conditional conjugate, exhibits reduced toxicity toward mammalian cells while conjugated, but
160 regains potent antibacterial activity once released by protease cleavage.

161 **Conditional calicheamicin conjugate demonstrates improved toxicity relative to free drug**
162 ***in vivo***

163 Having shown in vitro that conjugation masks calicheamicin's cytotoxicity and that
164 protease cleavage restores antibacterial activity, we next asked whether restricting activation to
165 the infection microenvironment reduces systemic, particularly hepatic, toxicity in vivo. To test
166 this, we compared the liver toxicity of the conditionally active calicheamicin conjugate with free
167 calicheamicin *in vivo*. Healthy mice were intravenously administered either free calicheamicin or
168 the conjugate (dose matched by drug concentration) (Fig. 2E). Liver injury was assessed 36 h
169 post-injection by measuring serum aspartate aminotransferase (AST) levels (Fig. 2F), alanine
170 aminotransferase (ALT) (Fig. 2G) and by histological analysis (Fig. S1). Mice treated with free
171 calicheamicin exhibited elevated AST (Fig. 2F) and ALT (Fig. 2G) levels. Mice receiving the
172 conjugate showed a significant reduction in toxicity relative to free drug, although serum liver
173 enzymes were significantly elevated above the baseline of mice treated with vehicle alone.

174 Histology revealed moderate to severe injury in mice treated with free drug, evidenced by
175 diffuse presence of hepatocytes with swollen cytoplasm or shrunken, hypereosinophilic cells
176 (Fig. S1) The livers of conjugate-treated mice showed more mild changes, including some
177 apoptotic cells with swollen cytoplasm, and some healthy cells, consistent with more limited
178 toxicity (Fig. S1). These findings indicate that formulation of calicheamicin as the conditionally-
179 active conjugate significantly reduces off-target hepatotoxicity *in vivo.*

180 **Microbial-derived antidotes can neutralize calicheamicin toxicity *in vitro* and *in vivo***

181 Formulation of calicheamicin as a conditional conjugate significantly reduced
182 hepatotoxicity in healthy mice but did not eliminate liver injury, which we hypothesized arose
183 from a fraction of drug released outside the infection site, potentially via low levels of protease-
184 mediated activation outside the infection environment, or diffusion of released drug from
185 infected tissue back into the bloodstream. We therefore developed a second complementary
186 strategy to address these residual sources of toxicity and further improve the safety profile of
187 calicheamicin. To achieve a second layer of toxicity mitigation, we drew inspiration from the
188 natural self-resistance mechanism of *Micromonospora echinospora*, the native producer of
189 calicheamicin, which avoids self-toxicity by enzymatically inactivating the compound. We
190 envisioned adapting this self-resistance strategy for therapeutic use by engineering long-
191 circulating variants of these calicheamicin-neutralizing enzymes to act as “antidotes”,
192 intercepting and neutralizing calicheamicin that escapes the infection microenvironment before it
193 reaches sensitive tissues (Fig. 3A).

194 We first evaluated which of the native self-resistance enzymes would be most suitable
195 for adaptation as a circulating antidote. The calicheamicin biosynthetic cluster encodes three
196 self-resistance enzymes, CalC, CalU16, and CalU19 (*21*, *22*). Reduction of calicheamicin’s
197 trisulfide bond generates the reactive species responsible for its cytotoxicity. CalC and CalU16

198 act only on this reduced form, whereas CalU19 also neutralizes the unreduced molecule,
199 making it best suited for calicheamicin neutralization in circulation, which is not a reducing
200 environment. We recombinantly expressed CalU19 and sought to confirm its neutralizing activity
201 *in vitro,* by evaluating if administration of CalU19 could protect mammalian cells from
202 calicheamicin-induced toxicity. HepG2 cells were incubated with serial dilutions of calicheamicin
203 in the presence or absence of a fixed concentration of CalU19 for 24 hours, and cell viability
204 was assessed by MTS assay (Fig. 3B). CalU19 conferred protection, with the highest protection
205 observed at lower calicheamicin concentrations, consistent with the stoichiometric mechanism
206 of inactivation in which one molecule of CalU19 is consumed per molecule of calicheamicin
207 neutralized (Fig. 3B).

208 Following *in vitro* validation of CalU19 activity, we next assessed its ability to selectively
209 neutralize free calicheamicin without affecting the conjugated drug. During calicheamicin
210 neutralization, CalU19 undergoes a unique self-cleavage event, which can be used as an
211 indicator of neutralizing activity. SDS-PAGE of CalU19 incubated with calicheamicin, ABD-Cal
212 or vehicle, revealed CalU19 self-cleavage fragments only when CalU19 was incubated with free
213 calicheamicin (Fig. S2), confirming that neutralizing activity is restricted to free drug.

214 To realize our design goal of a long-circulating antidote capable of soaking up off-target
215 drug *in vivo*, we next engineered CalU19x for *in vivo* administration. We first removed two
216 unpaired cysteines, which could promote off-target interactions with other proteins in vivo,
217 substituting them with alanine to generate CalU19x, which retained neutralizing activity
218 comparable to the wild-type enzyme (Fig. 3B). We then assessed CalU19 *pharmacokinetics in*
219 *vivo* (Fig. 3C, D). Fluorophore-labeled CalU19 and CalU19x were both rapidly cleared from
220 circulation, with plasma half-lives of ~1 h. To extend the circulation half-life of CalU19x, we
221 generated fusions to single (C-CalU19x) and tandem (LC-CalU19x) albumin-binding domains,
222 as these extend half-life through association with serum albumin. LC-CalU19x exhibited the

223 longest half-life, remaining detectable for at least 48 h in plasma (Fig. 3D), and maintained
224 neutralizing activity *in vitro* comparable to wild-type CalU19 (Fig. 3B).

225 Having established a long-circulating antidote *in vitro*, we next evaluated whether LC-
226 CalU19x could protect against calicheamicin toxicity *in vivo*. Healthy animals were intravenously
227 administered LC-CalU19x or vehicle followed by dosing with calicheamicin (Fig. 3E). Serum and
228 tissue were collected 36-48 h later, and serum AST and ALT levels were quantified. Mice
229 administered calicheamicin and LC-CalU19x showed significantly reduced serum AST (Fig. 3F)
230 and ALT (Fig. 3G) compared with mice administered calicheamicin and vehicle, indicating
231 mitigation of calicheamicin-induced hepatotoxicity. Histology (Fig. S3) agreed with these
232 findings: livers from mice administered calicheamicin and LC-CalU19x-treated mice were largely
233 indistinguishable from healthy controls, whereas mice treated with calicheamicin alone
234 displayed hepatocellular degeneration and necrosis, indicated by swollen cells with eosinophilic
235 cytoplasm (Fig. S3). Together, these results demonstrate that LC-CalU19x acts as a circulating
236 antidote that mitigates off-target toxicity without interfering with the activity of the conditionally-
237 active calicheamicin conjugate, supporting their use as a combined therapy.

238 **Calicheamicin conjugate and antidote combination achieves antimicrobial efficacy in**
239 **mouse models of pneumonia**

240 We proceeded to test the preclinical potential of ABD-calicheamicin conjugate and LC-
241 CalU19x in combination, evaluating whether co-administration of the antidote with the
242 conditionally-active drug would reduce bacterial burden, while minimizing liver toxicity in a mouse
243 model of bacterial pneumonia. Mice were infected with bacterial pathogen *S. aureus*, followed by
244 intratracheal administration of vehicle, ABD-calicheamicin alone, or ABD-calicheamicin in
245 combination with intravenously administered LC-CalU19x (Fig. 4A-B). Treatment of *S. aureus*-
246 infected mice with the conditionally-active conjugate and antidote resulted in a 4-log reduction in
247 lung bacterial burden 6 h after administration, compared with the vehicle control, demonstrating

248 that on-target antimicrobial efficacy is preserved in the presence of the antidote (Fig. 4B).
249 Comparing liver toxicity between mice treated with ABD-Cal alone or ABD-Cal with CalU19x, we
250 observed a significant reduction in toxicity for mice treated with conjugate and antidote relative to
251 the conjugate-only and vehicle groups, as measured by serum AST (Fig. 4C) and ALT (Fig. 4D),
252 with levels in the antidote-treated mice comparable to the untreated healthy control. Together,
253 these findings demonstrate that pairing a conditionally-active calicheamicin conjugate with a long-
254 circulating enzyme antidote maintains antimicrobial efficacy while substantially reducing systemic
255 toxicity.

256 **DISCUSSION**

257 In this work, we demonstrate two complementary strategies to expand the therapeutic
258 window of a chemotherapeutic drug, calicheamicin, drawing inspiration from 1) engineered
259 oncology approaches for managing toxic therapeutics and 2) natural microbial mechanisms for
260 detoxification. In oncology, antibody–drug conjugates (ADCs) take advantage of
261 microenvironmental cues to restrict payload activity to the site of disease; we created a
262 calicheamicin conjugate that restricts drug activation to infected tissue, reducing systemic
263 toxicity. In parallel, we take advantage of the natural self-resistance mechanism from the
264 calicheamicin producing organism, optimizing and then administering a calicheamicin-
265 neutralizing “antidote” to inactivate off-target free drug. The combination of conjugate and
266 antidote successfully treated bacterial pneumonia in mice while reducing hepatotoxicity,
267 demonstrating that the two complementary strategies, conditional activation and antidote co-
268 administration, can widen the therapeutic window of a potent cytotoxin.

269 Conditional drug conjugates hold considerable potential for infectious disease, but their
270 development in that context is far less common than in oncology, where antibody–drug
271 conjugates (ADCs) have achieved notable clinical success (*26*, *27*, *30*, *31*). The distinct
272 biological context of bacterial infections requires revising design criteria that have guided ADC

273 development in oncology. While oncology relies on antibodies to direct cytotoxic payloads to
274 defined tumor antigens, infection-focused conjugates would benefit from carrier proteins that
275 target the site of infection in an antigen-independent manner and are thus compatible with
276 broad-spectrum activity against a variety of pathogens. Our design (Fig. 2) uses an albumin-
277 binding domain (ABD) as our drug carrier, with the intent to promote retention (*28*) and
278 mucopenetration (*29*) at the sites of infection when administered into the lung. For the linker,
279 bacterial infection most likely will require extracellular drug release (except in the case of
280 intracellular pathogens), which is a heterogeneous environment, where disease-associated
281 triggers act amid variable pH and redox states in the presence of immune cells and cellular
282 debris. In contrast, ADCs for cancer typically exploit tumor-associated proteases such as
283 cathepsins to release payloads intracellularly within lysosomes, a defined environment with
284 acidic pH, reducing conditions, and a well-characterized protease repertoire (*32*). To achieve
285 robust and selective activation in this setting, we incorporated a peptide linker cleavable by
286 neutrophil elastase, which is enriched extracellularly at sites of bacterial infection after release
287 by recruited immune cells. The criteria for payload selection are consistent between the two
288 indications: potency is indispensable for efficacy. Early preclinical ADCs used conventional
289 chemotherapeutics with modest potency, which limited their efficacy (33). Recognition that
290 greater potency was required led to the development of gemtuzumab ozogamicin (Mylotarg),
291 the first FDA-approved ADC, which used calicheamicin as its payload. Although it achieved
292 strong clinical responses, its severe dose-limiting toxicities underscored the risks associated
293 with ultrapotent payloads (34). The use of calicheamicin in our conjugate therefore represents a
294 stringent test of whether such highly potent molecules can be safely repurposed for
295 antimicrobial use.

296 Formulation of calicheamicin as a conjugate reduced liver toxicity but did not fully
297 eliminate it (Fig. 2), consistent with both preclinical and clinical data from oncology. While

298 conditional drug conjugates have demonstrated clear clinical success (*33*), some evidence
299 suggests that the maximum tolerated doses of some ADCs approach those of the unconjugated
300 payload (*20*, *34–36*). Thus, ADCs improve efficacy but do not always reduce toxicity, and the full
301 therapeutic potential of this modality has not been realized. Prior efforts have focused on
302 refining the antibody, linker, or payload to reduce toxicity, but off-target damage in the liver,
303 bone marrow, and gastrointestinal tract remains a major barrier. To move beyond these
304 limitations in the context of infection, we turned to microbes themselves, which not only produce
305 some of the cytotoxic natural products used as ADC payloads but also encode self-resistance
306 enzymes to protect against autotoxicity. Inspired by this microbial strategy, we introduced a
307 second layer of protection: delivery of an engineered self-resistance enzyme derived
308 from *Micromonospora echinospora*, the natural producer of calicheamicin, as an antidote to
309 neutralize circulating free drug outside the site of infection (Fig. 3). While antibiotic adjuncts that
310 enhance antimicrobial activity are under development (*37–40*), coadministration of agents
311 specifically designed to mitigate host toxicity is less explored in infectious disease. This model is
312 under active consideration within oncology contexts, for example in preclinical work examining
313 neutralization of toxicity for radiation (*41*), and clinically in the use of dasatinib (*42*) to mitigate
314 cytokine release syndrome after administration of CAR-T therapy.

315 Despite the promise of our drug conjugate and antidote platform, several challenges
316 may remain before translation to clinical settings. Microbial-derived proteins like the antidote we
317 developed may be immunogenic upon repeated administration, as is often required in the
318 treatment of bacterial infections. Existing strategies such as PEGylation (*43*), domain
319 humanization (*44*), or epitope masking (*45*) could reduce immunogenic potential, and there are
320 encouraging examples of regulator-approved and clinically-used products derived from
321 microbial enzymes (*46*, *47*). Second, the success of this dual system hinges on spatial, kinetic,
322 or temporal separation between on-target activity and off-target detoxification. In our current

323 model, we achieve this using compartmentalization, via local pulmonary delivery of the drug
324 conjugate and systemic administration of the antidote (Fig 4). This separation is also achieved
325 by virtue of the conjugate, which protects the drug from premature neutralization by the antidote,
326 as the antidote can only bind and inactivate the released, active form of the drug (Fig. S2).
327 However, extending the paired conjugate-antidote system to other sites of infection will require
328 context-specific tailoring. For example, we hypothesize that treatment of systemic bloodstream
329 infections would likely require prophylactic delivery of CalU19, either as a protein or mRNA
330 encapsulated in lipid nanoparticles, such that they can be taken up by liver sinusoidal
331 endothelial cells or hepatocytes to protect these tissues prior to systemic administration and
332 release of calicheamicin from the conjugate in response to cues from the bloodstream infection.
333 The modularity of our platform, with the ability to exchange the carrier protein and linker within
334 the conjugate and the possibility of fusing other targeting partners to CalU19, to control half-life
335 or localization within the body, makes such adaptation feasible. Finally, the kinetics of enzyme-
336 mediated neutralization of “off-target” drug relative to bacterial uptake and killing by “on target”
337 drug remain incompletely understood. Future studies may benefit from structure-guided
338 engineering or directed evolution of CalU19 to modulate its catalytic efficiency to further
339 enhance the therapeutic window of the conjugate and antidote pair.

340 Beyond calicheamicin, our dual strategy—1) leveraging selective activity within the
341 infected microenvironment and (2) engineering of microbial resistance proteins as adjuncts to
342 neutralize off-target toxicity--offers a generalizable framework to rapidly mobilize other
343 promising but previously unusable compounds for antimicrobial development. The modular
344 nature of our system, which allows for the easy swapping of targeting moieties, linker and drug,
345 enables facile adaptation to varied infection contexts. Potentially valuable classes of compounds
346 for this dual strategy include cytotoxic therapeutics with narrow therapeutic indices, antibiotic
347 candidates that failed in late-stage clinical trials due to toxicity, and preclinical compounds

348 developed in pharmaceutical pipelines but later abandoned, due to toxicities and/or poor
349 pharmacokinetics, with eventual disinvestment by industry (*48–51*). By mobilizing such agents
350 with conditional activation and antidote-mediated neutralization, these candidates could be re-
351 evaluated with the advantage of an accelerated development timelines and reduced costs from
352 leveraging existing chemistry, pharmacology, and, in some cases, clinical data. Looking ahead,
353 genome mining and artificial intelligence could accelerate the discovery and prioritization of
354 naturally produced drug–antidote pairs, leveraging microbial self-resistance strategies such as
355 enzymatic inactivation or compound sequestration. Beyond mining natural mechanisms, these
356 same tools may also enable *de novo* design of antidotes, creating entirely new ways to widen
357 the therapeutic index.

358 More broadly, the combined use of the drug conjugate and antidote represents a
359 conceptual shift in antibiotic treatment—towards a form of molecular stewardship—in which
360 each molecule of the antimicrobial is accounted for, with on-target directed precisely to the site
361 of infection while off-target drug is actively neutralized. Although mitigation of liver toxicity was a
362 primary goal of this work, the same principle could reduce collateral damage to other sensitive
363 tissues, such as the bone marrow. Antibiotic-induced dysbiosis of the gut microbiome is another
364 major concern, such that antibiotic treatment is frequently associated with shifts in microbial
365 composition, overgrowth of opportunistic pathogens such as *Clostridioides difficile*, and impaired
366 gut barrier function (*52*, *53*). We hypothesize that co-administration of an antidote could
367 attenuate antibiotic-associated microbiome disruption by neutralizing drug before it reaches the
368 gastrointestinal tract. Beyond the host, excreted antibiotics that enter into the environment
369 through sewage and wastewater exert selective pressure on environmental bacteria, which can
370 drive the emergence of resistance through exposure to sublethal concentrations (*54*). The
371 excretion of highly potent cytotoxic compounds such as calicheamicin also raises concerns
372 about ecological toxicity (*55–57*). Incorporation of antidotes into therapeutic regimens may

373 therefore not only improve safety within the patient but also mitigate the broader ecological
374 consequences of antimicrobial use. Finally, outside of the context of infectious disease, we
375 envision antidotes as an enabling technology for conditionally-active conjugates more generally,
376 with the potential to mitigate toxicity in oncology and other therapeutic indications where potent,
377 conditionally-active drugs are administered.

378 **ACKNOWLEDGEMENTS, FUNDING AND COMPETING INTERESTS**

379 We are grateful to Dr. Laura Kiessling and Dr. Deborah Hung for their scientific insight and
380 support over the course of the work. We are grateful to the Koch Institute Swanson Biotechnology
381 Center, specifically the Histology core (Kathy Cormier, Magalie Boucher) and the Biopolymer and
382 Proteomics core (Heather Amoroso). We are grateful to Kasturi Chakraborthy, Susanna Elledge
383 and Vardhman Kumar for feedback on the manuscript. This work was supported by R01 AI132413
384 and U19 AI142780 grants from the National Institute of Allergy and Infectious Diseases. This
385 study was supported in part by the Koch Institute Support Grant P30-CA14051 from the National
386 Cancer Institute (Swanson Biotechnology Center) and Core Center Grant P30-ES002109 from
387 the National Institute of Environmental Health Sciences. Additional support was received from the
388 Koch Institute's Marble Center for Cancer Nanomedicine. This research was supported in part by
389 a generous gift from Joel Gantcher. T.S. was supported by a postdoctoral fellowship from the
390 Ludwig Center at MIT's Koch Institute for Integrative Cancer Research. S.N.B. is a Howard
391 Hughes Institute Investigator. Competing interests: S.N.B. reports consulting roles and/or equity
392 Amplifyer Bio, Catalio Capital, Danaher, Earli Inc., Impilo Therapeutics, Matrisome Bio, Ochre
393 Bio, Port Therapeutics, Satellite Bio, Sunbird Bio, and Xilio Therapeutics, which were not involved
394 in this study.

395

396 **MATERIALS and METHODS**

397 **Bacterial strains and culture**

398 *Escherichia coli* ATCC 29522, *Klebsiella pneumoniae* ATCC 43816, *Pseudomonas*
399 *aeruginosa* PAO1, *Staphylococcus aureus* 502A, and *Staphylococcus*
400 *aureus* USA300_FPR3757 were used in this study. Strains were obtained from the American
401 Type Culture Collection (ATCC) or as indicated. Bacteria were cultured in Mueller–Hinton broth
402 (MHB; BD Difco) at 37 °C with shaking at 250 r.p.m. Growth was monitored by optical density at
403 600 nm (OD600).

404 **Molecular cloning**

405 gBlock™ gene fragments encoding ABD with a C-terminal cysteine ($(ABD)_2$-$(EEG)_6$-Cys), CalC,
406 and CalU19 with flanking restriction sites NcoI and XhoI were ordered from Integrated DNA
407 Technologies, cloned into pET28(a) by restriction enzyme digestion and ligation, and transformed
408 into *E. coli* DH5α competent cells (New England Biolabs). Colonies encoding the correct inserts
409 were confirmed by Sanger sequencing (QuintaraBio), and plasmids were purified using a plasmid
410 miniprep kit (Thermo Fisher Scientific). For CalU19 variants, clonal genes were directly obtained
411 from Twist Bioscience already cloned into the pET28(a) expression vector. All expression
412 plasmids were subsequently transformed into *E. coli* BL21(DE3) cells for protein expression.
413

414 **Protein expression**

415 A secondary culture (500 mL LB broth (50 µg/mL kanamycin)) of *E coli.* BL21(DE3) encoding the
416 protein of interest was expanded from an overnight primary culture (3 mL) in an incubator shaker
417 at 37 °C until OD600 reached about 0.6 (~ 4hours). Protein expression was induced by addition
418 of an IPTG solution to a final concentration of 1 mM. The induced culture was incubated in an
419 incubator shaker for 2 h at 37 °C after which the culture was centrifuged and the bacteria pellet
420 was frozen and stored in a -80 °C freezer. For purification, the bacteria pellet was thawed in a 37
421 °C water bath and lysed with a B-PER™ complete bacterial protein extraction reagent

422 (ThermoFisher). The lysed solution was centrifuged and the supernatant was incubated with
423 Qiagen Ni-NTA agarose for 30minutes at 4 °C to capture the product. The agarose was
424 transferred to a fritted column, washed sequentially with a wash buffer A (50 mM Tris, 500 mM
425 NaCl, 2% Triton X-114) (10 column volumes (CVs)) and a wash buffer B (50 mM Tris, 500 mM
426 NaCl) (10 column volumes) before elution with an elution buffer (500 mM imidazole, 50 mM Tris,
427 500 mM NaCl, 10% glycerol) (3 CVs). The purified protein was confirmed via SDS-PAGE analysis
428 with Coomassie blue staining.
429
430 **Synthesis of Conjugate Azide-AAPV-calicheamicin**
431 An N-terminal azidoacetylated peptide substrate with a C-terminal penicillamine (Pen) (Azide-
432 AAPV-Pen) was synthesized by CPC Scientific via a standard Fmoc-based solid phase peptide
433 synthesis. A solution of calicheamicin (1 eq.) (MedChemExpress) in N,N-dimethylformamide
434 (DMF) was added to a solution of Azide-AAPV-Pen (3 eq.) in DMF followed by addition of
435 triethylamine (8 eq.) to the reaction solution. The reaction solution was purged with nitrogen for
436 5minutes and incubated for 24hours at 4 °C. The Azide-AAPV-calicheamicin product was purified
437 by the Koch Institute Biopolymers & Proteomics core facility using a semi-preparative HPLC
438 column and confirmed with MALDI-ToF MS.
439 $(ABD)_2$-$(EEG)_6$-Cys was incubated with TCEP (10 eq.) for 30minutes at RT and buffer-exchanged
440 into PBS (1 mM EDTA, pH 6.5) using an Amicon 10-kDa, ultra-0.5 centrifugal filter unit (14,000
441 rpm, 2minutes, 4 times). The reduced protein was incubated with DBCO-Maleimide (4 eq.) for
442 4hours at RT. The ABD-DBCO product was purified and buffer-exchanged into PBS using a PD-
443 10 desalting column (Cytiva).
444 *Synthesis of ABD-calicheamicin conjugates*
445 Azide-Sx-calicheamicin (2 eq.) was dissolved in DMF and added to a solution of ABD-DBCO (1
446 eq.) in PBS to a final concentration of 50% DMF. The reaction solution was incubated for 24hours
447 at RT and centrifuged to remove precipitate. The product in supernatant was immobilized on Ni-

448 NTA agarose, washed with a wash buffer C (50 mM Tris, 500 mM NaCl, 20% DMF) (10 CVs) and
449 a wash buffer B (10 CVs) before elution with the elution buffer. The product was buffer-exchanged
450 into PBS using a PD-10 desalting column and quantified via absorbance at 200 nm. The product
451 was confirmed and assessed for percentage purity using SDS-PAGE analysis.

452 ***In vitro* activity and toxicity masking**

453 To evaluate conditional activation, ABD–calicheamicin conjugates were incubated with
454 recombinant human neutrophil elastase (Enzo Life Sciences) or vehicle control in PBS at 37 °C
455 for 4 h. Reaction mixtures were then diluted into bacterial or mammalian assay media as
456 described below. Minimum inhibitory concentrations (MICs) were determined in accordance with
457 CLSI guidelines. Briefly, bacteria were seeded at OD 0.005 in 96-well plates containing MHB
458 supplemented with conjugate, protease-treated conjugate, or controls. Plates were incubated at
459 37 °C for 24 h, and bacterial growth was assessed by measuring optical density at 600 nm
460 (SpectraMax i3, Molecular Devices). MICs were defined as the lowest concentration of
461 conjugate preventing visible bacterial growth. Human hepatocellular carcinoma cells (HepG2,
462 ATCC HB-8065) were maintained in Dulbecco's Modified Eagle Medium (DMEM; Thermo
463 Fisher Scientific) supplemented with 10% fetal bovine serum (FBS) and 1% penicillin–
464 streptomycin. For cytotoxicity assays, HepG2 cells were seeded at 1 × 10^4 cells per well in
465 collagen-coated 96-well plates and allowed to adhere overnight. Cells were then exposed to
466 intact or protease-treated ABD–calicheamicin conjugates for 24 h. Viability was quantified using
467 the CellTiter AQueous MTS assay (Promega) according to the manufacturer's instructions, and
468 absorbance was read at 490 nm using a plate reader. In vitro activity and toxicity data were fit
469 using a four-parameter logistic (4PL) sigmoidal model, where X represents concentration, in
470 GraphPad Prism (GraphPad Software).

471

472 ***In vitro* CalU19 neutralization evaluation**

473 *SDS-PAGE* CalU19 was labeled with Cy7 through random lysine labeling and incubated with
474 vehicle, calicheamicin, or ABD-Cal for 4 hours at 37C. At 4h, reactions were run on a gel
475 (NuPAGE™ 4-12% Bis-Tris Protein Gels, 1.0 mm, 12-well, Thermofisher) which was then
476 imaged using an Odyssey CLx imager in the 800 nm channel, for detection of Cy7 fluorescence,
477 monitoring specifically for the presence of the intact protein at ~27 kDa, as well as the self-
478 cleavage fragments at 6kDa and 21 kDa.

479 *Cytotoxicity Assay* HepG2 cells were seeded at 1 × 10^4 cells per well in collagen-coated 96-
480 well plates and allowed to adhere overnight. Cells were then exposed to serial dilutions of
481 calicheamicin, in the presence of absence of 5 μM CalU19, CalU19x, C-CalU19X, LC-CalU19x,
482 or vehicle (for the control). Viability was quantified at 24 h using the CellTiter AQueous MTS
483 assay (Promega) according to the manufacturer's instructions, and absorbance was read at 490
484 nm using a plate reader. Data were fit using a four-parameter logistic (4PL) sigmoidal model,
485 where X represents concentration, in GraphPad Prism (GraphPad Software).

486 ***In vivo* pharmacokinetics, activity and toxicity evaluation**

487 All animal studies were approved by the Massachusetts Institute of Technology's Committee on
488 Animal Care (MIT CAC protocol 2203000310). For infected mice, bacterial inocula were
489 prepared from mid-logarithmic phase cultures grown in Mueller–Hinton broth, washed twice with
490 PBS, and quantified by optical density and serial dilution plating. Following administration, mice
491 were monitored continuously until recovery from anesthesia and then observed at regular
492 intervals for clinical signs of infection, including weight loss, respiratory distress, and reduced
493 activity. For lung infections, CD-1 mice (10-12 weeks old) were administered 1.25 x 10^8 CFU of
494 *S. aureus* (502A) (suspended in PBS) by intratracheal administration using a 22G blunt end

495 catheter and monitored after administration. At designated time points post-infection, mice were
496 euthanized, lungs were aseptically harvested, and/or blood was collected.

497 *CFU quantification* Lungs were weighed and homogenized in sterile PBS using gentleMACS M-
498 tubes (Miltenyi Biotec). Homogenates were serially diluted and plated on mannitol salt agar (BD
499 Difco) to selectively recover *S. aureus*, with colonies were enumerated after 24 h incubation at
500 37 °C.

501 *Histology* Lungs were fixed in 10% neutral buffered formalin for at least 48 h, processed, and
502 paraffin-embedded by the Koch Institute Histology Core Facility. Tissue sections (X µm) were
503 stained with hematoxylin and eosin (H&E) and imaged using brightfield microscopy. Histological
504 evaluation was performed by

505 *Toxicity evaluation* To evaluate liver toxicity, blood was collected from mice at designated time
506 points via terminal cardiac puncture. Whole blood was allowed to clot at room temperature in
507 BD Microtainer SST tubes with gold tops (BD Biosciences, Cat. No. 365967). The resulting
508 serum was aliquoted and stored at –80 °C until analysis. Serum alanine aminotransferase (ALT)
509 activity was quantified using a colorimetric assay kit (Thermo Fisher Scientific, ALT/GPT Activity
510 Assay Kit, Cat. No. EEA001, and serum aspartate aminotransferase (AST) activity was
511 measured using a colorimetric assay kit (MilliporeSigma, AST Activity Assay Kit, Cat. No.
512 MAK055), following the manufacturers' protocols. Absorbance was read using a microplate
513 reader (SpectraMax i3, Molecular Devices).

514 *Pharmacokinetics* CalU19 variants were conjugated with Cy7 through random lysine labeling.
515 Labeled proteins were administered intravenously to CD-1 mice. At the indicated time points,
516 blood was collected from the tail vein using heparinized capillary tubes, diluted in PBS
517 containing EDTA, and centrifuged to remove cells. Fluorescence in plasma supernatants was

quantified using a microplate reader to determine circulating protein concentrations. Percentage of antidote protein remaining in circulation was calculated as the percentage of antidote at each timepoint relative to the 1 min timepoint.

Statistical Analysis and Schematic Representation

Statistical analyses was performed with GraphPad Prism. Data are plotted as mean ± SD. Comparisons among different treatment groups are based on one-way ANOVA with Tukey *post hoc* tests. A P value < 0.05 was considered statistical significance. Parts of the schematics in this publication were created with BioRender.

REFERENCES

1. M. Naghavi *et al.*, *The Lancet*. **404**, 1199–1226 (2024).
2. C. Årdal *et al.*, *Nat Rev Microbiol*. **18**, 267–274 (2020).
3. F. Ruggieri *et al.*, *European Journal of Medicinal Chemistry*. **256**, 115413 (2023).
4. G. Liu *et al.*, *Nat Chem Biol*. **19**, 1342–1350 (2023).
5. F. Wan, F. Wong, J. J. Collins, C. de la Fuente-Nunez, *Nat Rev Bioeng*. **2**, 392–407 (2024).
6. C. D. Santos-Júnior *et al.*, *Cell*. **187**, 3761-3778.e16 (2024).
7. F. Wong, C. de la Fuente-Nunez, J. J. Collins, *Science*. **381**, 164–170 (2023).
8. N. K. Khandelwal *et al.*, *Nat Commun*. **16**, 3139 (2025).
9. M. W. Tse *et al.*, *Proc Natl Acad Sci U S A*. **122**, e2402017122 (2025).
10. M. D. T. Torres *et al.*, *Cell*. **187**, 5453-5467.e15 (2024).
11. W. Liang, J. Diana, *EMBO Mol Med*. **14**, e15409 (2022).
12. M. Chawla, J. Verma, R. Gupta, B. Das, *Front. Microbiol.* **13** (2022), doi:10.3389/fmicb.2022.887251.
13. B. Bognár, R. Spohn, V. Lázár, *npj Antimicrob Resist*. **2**, 1–8 (2024).
14. Z. Si, K. Pethe, M. B. Chan-Park, *JACS Au*. **3**, 276–292 (2023).

15. M. A. Farha, E. D. Brown, *Nat Microbiol*. **4**, 565–577 (2019).

16. E. Mitchell *et al.*, *Nat Genet*. **57**, 1684–1694 (2025).

17. G. Cavaletti, *Nat Rev Cancer*. **8**, 72–72 (2008).

18. M. E. McNerney, L. A. Godley, M. M. Le Beau, *Nat Rev Cancer*. **17**, 513–527 (2017).

19. F. J. Giles *et al.*, *Cancer*. **92**, 406–413 (2001).

20. M. Guffroy *et al.*, *Clin Cancer Res*. **23**, 1760–1770 (2017).

21. J. B. Biggins, K. C. Onwueme, J. S. Thorson, *Science*. **301**, 1537–1541 (2003).

22. S. I. Elshahawi *et al.*, *ACS Chem Biol*. **9**, 2347–2358 (2014).

23. WHO bacterial priority pathogens list, 2024: Bacterial pathogens of public health importance to guide research, development and strategies to prevent and control antimicrobial resistance, (available at https://www.who.int/publications/i/item/9789240093461).

24. E. L. Sievers *et al.*, *Blood*. **93**, 3678–3684 (1999).

25. E. L. Sievers *et al.*, *J Clin Oncol*. **19**, 3244–3254 (2001).

26. C. Ngambenjawong, L. W. Chan, H. E. Fleming, S. N. Bhatia, *ACS Nano*. **16**, 15779–15791 (2022).

27. C. Ngambenjawong *et al.*, *ACS Nano*. **19**, 9958–9970 (2025).

28. L. W. Chan *et al.*, *Nat. Nanotechnol.* **15**, 792–800 (2020).

29. K. Rakhra *et al.*, *Science Immunology*. **6**, eabd8003 (2021).

30. S. M. Lehar *et al.*, *Nature*. **527**, 323–328 (2015).

31. K. K. Kajihara *et al.*, *mBio*. **12**, e00202-21.

32. J. D. Bargh, A. Isidro-Llobet, J. S. Parker, D. R. Spring, *Chem. Soc. Rev.* **48**, 4361–4374 (2019).

33. K. Liu *et al.*, *Molecular Cancer*. **23**, 62 (2024).

34. R. Colombo, J. R. Rich, *Cancer Cell* (2022), doi:10.1016/j.ccell.2022.09.016.

35. H.-P. Gerber, S. Gangwar, A. Betts, *MAbs*. **15**, 2230618.

36. J. E. Fisher, *Antibodies (Basel)*. **10**, 15 (2021).

37. J. Joseph, S. Boby, S. Mooyottu, M. S. Muyyarikkandy, *npj Antimicrob Resist*. **3**, 53 (2025).

38. C. Reading, M. Cole, *Antimicrob Agents Chemother*. **11**, 852–857 (1977).

39. J. M. Stokes *et al.*, *Nat Microbiol*. **2**, 17028 (2017).

40. N. Blondiaux *et al.*, *Science*. **355**, 1206–1211 (2017).

41. A. R. Kirtane *et al.*, *Nat. Biomed. Eng*. **9**, 1240–1253 (2025).

42. K. Mestermann *et al.*, *Science Translational Medicine*. **11**, eaau5907 (2019).

43. J. M. Harris, R. B. Chess, *Nat Rev Drug Discov*. **2**, 214–221 (2003).

44. P. J. Carter, A. Rajpal, *Cell*. **185**, 2789–2805 (2022).

45. L. V. Zinsli, N. Stierlin, M. J. Loessner, M. Schmelcher, *Comput Struct Biotechnol J*. **19**, 315–329 (2021).

46. A. E. Place *et al.*, *Lancet Oncol*. **16**, 1677–1690 (2015).

47. L. C. Hurst *et al.*, *New England Journal of Medicine*. **361**, 968–979 (2009).

48. N. K. Prasad, I. B. Seiple, R. T. Cirz, O. S. Rosenberg, *Antimicrobial Agents and Chemotherapy*. **66**, e00054-22 (2022).

49. L. J. V. Piddock, R. Malpani, A. Hennessy, *ACS Infect. Dis.* **10**, 2445–2447 (2024).

50. U. Theuretzbacher, K. Outterson, A. Engel, A. Karlén, *Nat Rev Microbiol*. **18**, 275–285 (2020).

51. L. L. Silver, *Clin Microbiol Rev*. **24**, 71–109 (2011).

52. J. de la Cuesta-Zuluaga, L. Boldt, L. Maier, *Cell Host & Microbe*. **32**, 786–793 (2024).

53. B. P. Willing, S. L. Russell, B. B. Finlay, *Nat Rev Microbiol*. **9**, 233–243 (2011).

54. D. G. J. Larsson, C.-F. Flach, *Nat Rev Microbiol*. **20**, 257–269 (2022).

55. Fate and effects of cytostatic pharmaceuticals in the environment and the identification of biomarkers for and improved risk assessment on environmental exposure | FP7. *CORDIS | European Commission*, (available at https://cordis.europa.eu/project/id/265264/reporting).

56. A. Castellano-Hinojosa, M. J. Gallardo-Altamirano, J. González-López, A. González-Martínez, *J Hazard Mater*. **447**, 130818 (2023).

57. S. Mukherjee, D. Mehta, K. Dhangar, M. Kumar, *Chemical Engineering Journal*. **407**, 127184 (2021).

601 **FIGURES AND TABLES**

602

Table 1

	Calicheamicin γ1
Pseudomonas aeruginosa PAO1	0.11 μg/mL (78.1 nM)
Escherichia coli KS1	0.013 μg/mL (9.23 nM)
Klebsiella pneumoniae ATCC43816	0.05 μg/mL (312.5 nM)
Staphylococcus aureus 502A*	0.00061 μg/mL (835 pM)
BA1566 (MRSA)	0.00061 μg/mL (835 pM)

*For comparison, MIC of vancomycin for SA 502A was measured as 1 μg/mL

Table 1 Antibacterial activity of calicheamicin against representative Gram-negative and Gram-positive pathogens.
Minimum inhibitory concentrations (MICs) were determined by microdilution assay in Mueller–Hinton medium supplemented with 3% DMSO. Data represent biological triplicates.

603

604

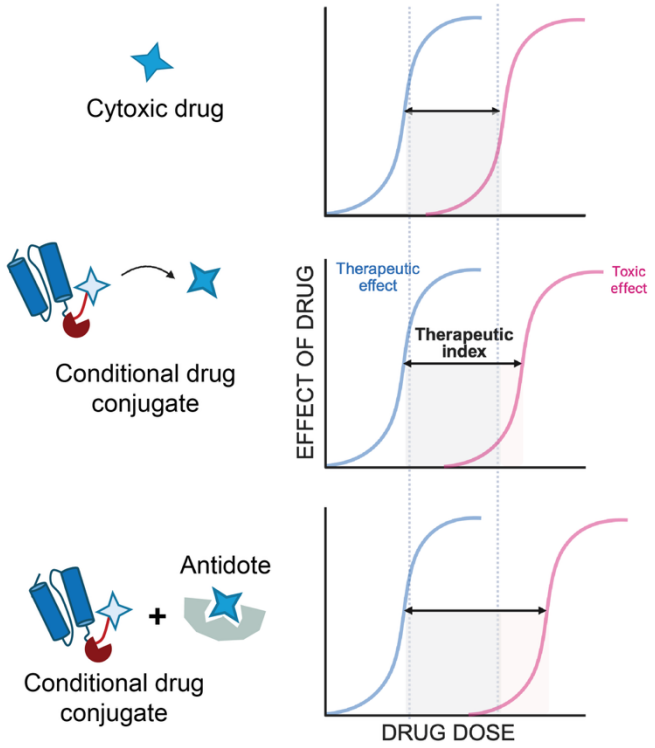

Figure 1. Dual strategy to expand the therapeutic index of toxic compounds for antimicrobial use. (Top) A narrow therapeutic index, defined as the difference between the median therapeutic effect and the median toxic effect, constrains the utility of cytotoxins (blue star) as antimicrobials. (Middle) Formulation of cytotoxins as conditionally active conjugates can widen the therapeutic index by restricting drug activity to an infection site, where proteases (red pac-man) release drug from the conjugate. (Bottom) “Antidotes” derived from self-resistance enzymes further widen the therapeutic index by neutralization off-target drug.

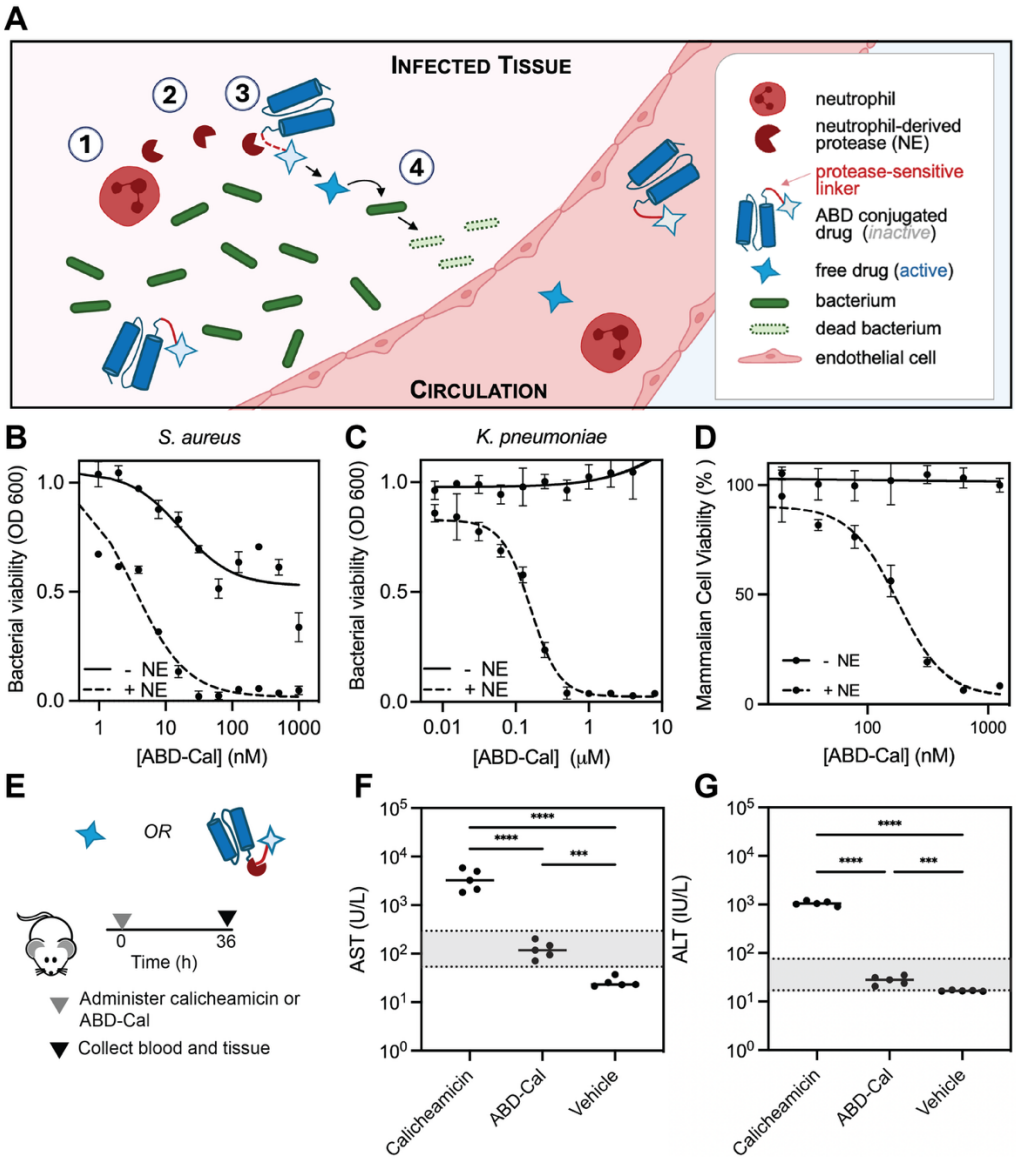

605

Figure 2. ABD-calicheamicin conjugate demonstrates masked mammalian toxicity and protease-triggered antibacterial activity *in vitro* and improved mammalian toxicity *in vivo.* (A) Schematic of ABD-calicheamicin conjugate (ABD-Cal) activation within the infection microenvironment. Within the infection environment, 1) neutrophils are recruited and 2) secrete neutrophil elastase which 3) cleaves and releases calicheamicin from the conjugate 4) such that it can kill bacteria. (B-C) Antimicrobial activity of ABD-Cal evaluated via microdilution assays against representative (B) Gram-positive and (C) Gram-negative bacterial strains in the presence or absence of recombinant neutrophil elastase. Bacterial growth measured by absorbance at 600 nm and normalized to untreated controls. Fold change in antimicrobial activity calculated as the ratio of MIC values of intact vs. cleaved conjugates. (mean ± sd, n = 3 biological replicates) (D) Masked mammalian toxicity of ABD-Cal evaluated via MTS cell proliferation assay in HepG2 cells. Cell viability measured by absorbance at 490 nm and normalized to untreated controls. Fold change in cytotoxicity calculated as the ratio of IC_{50} values of intact vs. cleaved conjugates. (mean ± sd, n = 3 biological replicates) (E) Schematic of experimental timeline of mice administered free calicheamicin (0.025 mg/kg) compared with ABD-Cal (0.025 mg/kg drug eq.) (F) Serum AST and (G) ALT. Dashed lines indicate normal healthy range. (n = 5 biological replicates. Statistical significance was determined by one-way ANOVA followed by Tukey's post hoc test). *P < 0.001* (***); *P* < 0.0001 (****)

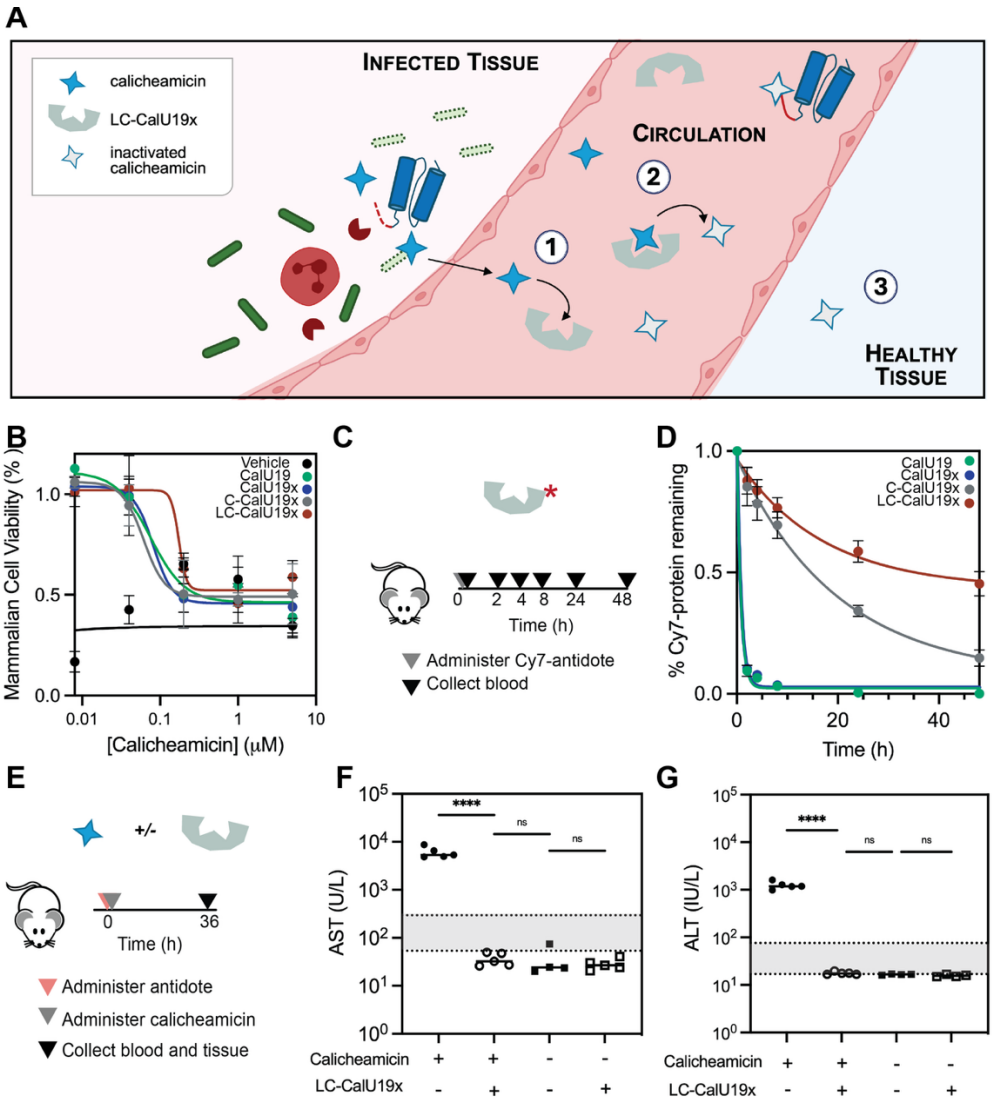

606

Figure 3. Microbial-inspired antidotes protect against calicheamicin-mediated liver toxicity *in vitro* and *in vivo.* Schematic illustrating neutralization of calicheamicin by engineered microbial self-resistance enzymes ("antidotes"). After neutrophil-elastase–mediated cleavage of the ABD–calicheamicin conjugate, either on-target (within the infection microenvironment) or off-target (within healthy tissue) released calicheamicin can 1) enter circulation, where it is 2) bound and inactivated by LC-CalU19x, such that exposure of healthy tissue to active drug is reduced. (B) Calicheamicin neutralization by engineered variants of CalU19 (evaluated via cell proliferation assay in HepG2 cells. Cell viability measured by absorbance at 490 nm and normalized to untreated controls. mean ± sd, n = 4 biological replicates. (C) Schematic of timeline during which Cy7-conjugated proteins were assayed for clearance from plasma. (D) Pharmacokinetics of antidote variants following systemic injection, with plasma concentrations of Cy7 quantified over time. (mean ± sd, n = 4–5 mice per group) (E) Schematic of *in vivo* neutralization of free calicheamicin by LC-CalU19x. (F) Serum AST and (G) ALT levels measured 36 h after calicheamicin administration with or without antidote treatment. Dashed lines indicate normal healthy range (n = 5 Statistical significance determined by one-way ANOVA followed by Tukey's post hoc test.) $P < 0.0001$ (****); ns: not significant.

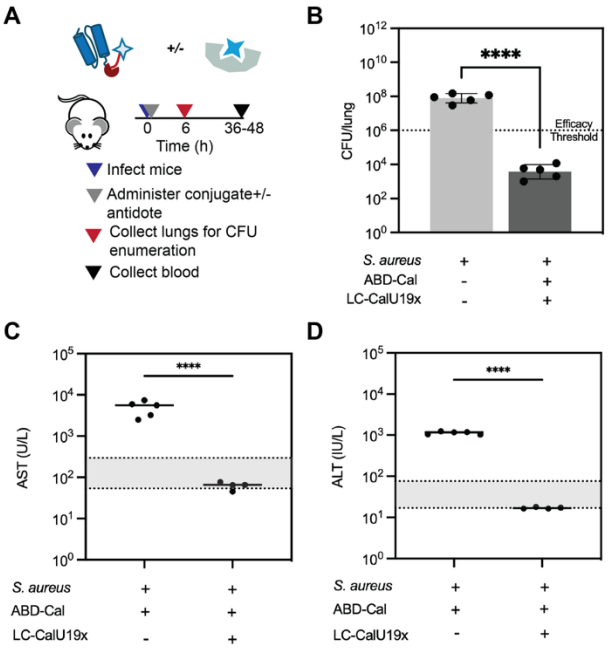

607

Fig. 4 Therapeutic efficacy of calicheamicin conjugate and neutralizing antidote in a murine model of bacterial pneumonia. (A) Schematic of experimental timeline. (B) Bacterial burden in lungs 6 h post-treatment in mice infected intratracheally with *Staphylococcus aureus* 502A and treated intratracheally with vehicle or conjugated calicheamicin (ABD-Cal) and then intravenously with vehicle or antidote (LC-CalU19x). Each point represents an individual animal (n = 5 per group) Statistical significance was determined by unpaired two-tailed *t*-test. (C) Serum levels of AST and (D) ALT measured 36-48 h after infection and treatment with ABD-Cal, in the presence or absence of antidote. Each point represents an individual animal (n = 4–5 per group). Dashed lines indicate the normal healthy range. Statistical significance was determined by unpaired t-test. $P < 0.0001$ (****)

608 **SUPPLEMENTARY FIGURES**

609 Figure S1. H&E-stained liver sections from mice receiving calicheamicin vs. ABD–Cal

610 Figure S2. CalU19 neutralizes free calicheamicin but not ABD-Cal

611 Figure S3. H&E-stained liver sections from mice receiving calicheamicin with or without LC-

612 CalU19x.

613